 FDMP, vol.5, no.4, pp.331-343, 2009

Numerical and Experimental Study of Forced Mixing with Static Magnetic Field on SiGe System

N. Armour[1] **and S. Dost**[1,2]

Abstract: A combined numerical and experimental investigation has been undertaken to explore the benefits of an applied static magnetic field on Silicon transport into a Germanium melt. This work utilized a similar material configuration to that used in the Liquid Phase Diffusion (LPD) and Melt-Replenishment Czochralski (Cz) growth systems.

The measured concentration profiles from the samples processed with and without the application of magnetic field showed very similar shape. The amount of silicon transport into the melt is slightly higher in the samples processed under magnetic field, and there is a substantial difference in dissolution interface shape indicating a change in flow structure. Without magnetic field, a flat stable interface is observed. In the presence of an applied field, however, the dissolution interface remains flat in the center but dramatically curves back into the source material near the wall. This indicates a far higher dissolution rate at the edge of the silicon source.

The 3-D numerical simulation results verify these observations and show that the flow structure of the melt has dramatically changed under the effect of magnetic field. Magnetic field-driven circulation cells develop at the edge of the melt increasing dissolution from this area. The change in the flow field is reflected in the concentration field, and consequently the transport of silicon into the melt is increased along the crucible wall.

Keywords: Diffusion, mixing, dissolution, growth from solution, germanium silicon alloys, semiconducting silicon alloys

Nomenclature

B	applied magnetic field intensity in kGauss
D_{Si}	diffusion coefficient of silicon species
σ_E	electric conductivity of the liquid phase

[1] Crystal Growth Laboratory, University of Victoria, Victoria, BC Canada V8W 3P6.
[2] Corresponding Author: E-mail: sdost@me.uvic.ca, Tel: +1 250 721 8898, Fax: +1 250 721 6294.

v	flow velocity vector
v_θ	flow circumferentail velocity component
v_r	flow radial flow velocity component
v_z	flow vertical velocity component
∇, ∇^2	Gradient and Laplacien operators in cylindrical coordinates, respectively
g	gravitational constant
ρ_L	mass density of the liquid phase
p	pressure
c	silicon mass fraction
c_{Si}	silicon initial mass fraction
γ_L	specific heat of the liquid phase
β_c	solutal expansion coefficient
T	temperature
k_L	thermal conductivity of the liquid phase
t	time
$\mathbf{f}_b$	total body force
$\mathbf{n}$	unit normal vector
$\mathbf{e}_r, \mathbf{e}_\theta, \mathbf{e}_z$	unit vectors in the radial, circumferential, and vertical directions, respectively
μ	viscosity of the liquid phase

1 Introduction

There has been recent interest in Silicon Germanium, Si_xGe_{1-x}, as an emerging semiconductor material since it possesses full miscibility across its composition range allowing for adjustment of the band gap and lattice parameter (Kasper(1995)). Bulk crystals of Si_xGe_{1-x} have application in photodetection, photovoltaics, thermal imaging, and as a substrate for Si_xGe_{1-x} epitaxial layers (Usami, Kitamura, Obara, Nose, Shishido, and Nakajima (2005)). The bulk Si_xGe_{1-x} substrates can be lattice-matched to the device layer, reducing strain. Among device structures of interest, the heterobipolar transistor has been most studied due to its applications in telecommunications. As for other important applications for Si_xGe_{1-x}, modulation doped field effect transistors and 1.3μm optoelectronics can be identified (Schuppen and Dietrich(1995)).

There are a number of crystal techniques used for the growth of single crystal Si_xGe_{1-x} alloys. The Czochralski (Cz) crystal growth technique is currently the most efficient method for producing bulk Si_xGe_{1-x} crystals. However, since the liquidus and solidus lines in the Si_xGe_{1-x} phase diagram are widely separated, pro-

ducing compositionally uniform material requires that silicon be replenished during growth from the melt (Yonega(2005)). Similarly in Bridgman growth of Si_xGe_{1-x} alloys, the transport of the species and the changing composition of the melt are again important for producing compositionally uniform crystals (Volz, Schweizer, Kaiser, Cobb, Vujisic, Motakef, and Szofran(2002); and Volz, Walker, Schweizer, Cobb, and Szofran(2005)). Liquid Phase Diffusion (LPD) is a solution growth technique used for Si_xGe_{1-x} growth. In LPD an applied thermal gradient drives silicon diffusion across the germanium melt to initiate growth, and uniform transport across the growth cell is required for homogeneous growth in this technique (Yildiz, Dost, and Lent(2005)).

In these systems the silicon source is placed at the top of the melt, and silicon feed material dissolves into a germanium melt in the opposite direction to the gravity-induced buoyancy force. Due to the large density difference between the silicon solute and the germanium-rich melt, the lighter silicon solute is buoyant, and acts as stabilizer in the melt against natural convection. This makes the silicon transport in these systems diffusion dominated, and naturally leads to slower growth rates.

As a continuation of the dissolution experiments performed earlier (Armour, Dost, and Lent(2007); Armour and Dost(2007, 2009)) along with further dissolution experiments we have performed a numerical analysis of the dissolution process under a vertical static applied magnetic field to examine the effect of the applied magnetic field (8 kGauss) on the flow structure in the melt. The effect of the magnetic field on flow can be controlled through the strength of the applied field. It is hoped that this type of forced mixing could be beneficial in optimizing LPD and Melt-Replenishment Czochralski growth of Si_xGe_{1-x}.

The effect of an applied magnetic field (static of rotating) on the melt flows depends on the characteristics of the system such as densities of the components of the melt, the electric conductivity of the melt, the level of applied temperature gradients, the geometry, etc. Static fields provide suppression where the convective flows are strong and rotating fields provide forced mixing changing the flow structures of the melt. Magnetic fields have been utilized in all methods of crystal growth to optimize growth with varying effects (a rich list of references can be found in Dost and Lent(2007)).

2 Experimental procedure

The experiments were conducted in a three zone vertical DC resistance tube furnace under isothermal conditions which were maintained over the crucible length at 1100°C. The materials were contained in a quartz crucible. The silicon used was single crystal optical grade, 5N material. The germanium used was 6N mate-

rial. The silicon and germanium were both cleaned and etched prior to loading into the crucible. The cleaning, etching and loading took place in a cleanroom environment. Once the materials were loaded, the crucible was evacuated to approximately $1x10^{-3}$ Pa. The crucible was then sealed with a hydrogen torch.

The crucible, pictured in Fig.1a, was hung in the furnace on a stainless steel rod. It was first preheated for approximately 1 hour above the hot zone at approximately 800˚C. To start the experiment, the crucible was dropped into the isothermal area (at 1100˚C) of the furnace from the preheating position. It was allowed to remain there for the selected experiment time (durations of 10, 20 or 30 minutes were selected). At the conclusion of the experimental time, the crucible was pulled from the furnace and quickly quenched in ice-water.

The samples were then sectioned axially into two bulk halves and a 2mm thick center slice. All pieces were polished for analysis. One bulk section was differentially etched to reveal structure. The etch used was a 4:1:1, H_2O:H_2O_2:HF solution. The center slice was used for the energy-dispersive X-ray spectrometry (EDS) compositional analysis on a SEM.

3 Simulation model and numerical procedure

Computational domain is shown in Fig.1b. 3-D numerical simulations were carried out using the commercial CFX 11 software package. Issues with the treatment of strong body forces in the software required the use of scaled body forces to allow convergence. In this scaled model the relative strengths of the magnetic and gravitational body forces were maintained. As we will see from the computational results, the scaled model shows trend of behavior and good correlation with experimental results.

An unstructured mesh was used over all the computation domains. A coarse mesh was used in the solid domains where only the energy transport equation was solved. A finer mesh was used over the liquid domain. This was required to achieve mesh independence in the velocity field and concentration field.

3.1 Field equations of the liquid phase

In the model we assume that the Ge-Si melt is an incompressible, Newtonian binary liquid mixture. We also assume that the well-known Boussinesq approximation holds, i.e., density changes are included only in the gravitational body force term and the density of the mixture is taken constant everywhere else. Under these conditions the field equations in the liquid domain, namely the equations of continuity, mass transport, momentum balance, and energy are given respectively by

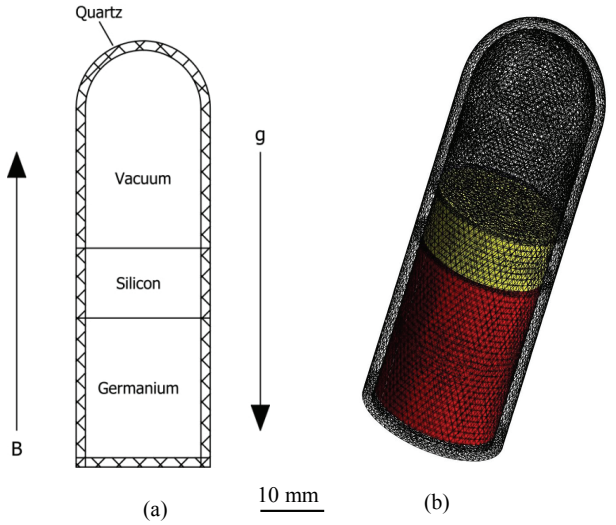

Figure 1: The diagram on the left (a) shows the experimental setup for the experiments. This geometry was replicated for the numerical simulation. The simulation grid is shown on the right (b). The quartz, silicon and vacuum domains were only used for the thermal analysis and as such only the energy transport equation was solved across these domains. The germanium melt was treated as the liquid domain where the field equations were solved numerically. Diameter of the ampoule is 24 mm.

Yildiz and Dost (2007):

$$\nabla \cdot \mathbf{v} = 0 \tag{1}$$

$$\frac{\partial c}{\partial t} + \mathbf{v} \cdot \nabla c = D_{Si} \nabla^2 c \tag{2}$$

$$\rho_L \{ \frac{\partial \mathbf{v}}{\partial t} - \mathbf{v} \times (\nabla \times \mathbf{v}) + \frac{1}{2} \nabla (\mathbf{v} \cdot \mathbf{v}) \} = -\nabla p + \mu \nabla^2 \mathbf{v} + \mathbf{f}_b \tag{3}$$

$$\frac{\partial T}{\partial t} + \mathbf{v} \cdot \nabla T = \frac{k_L}{\rho_L \gamma_L} \nabla^2 T \tag{4}$$

where the total body force $\mathbf{f}_b$ that consists of the buoyancy and magnetic body force components is taken as

$$\mathbf{f}_b = -\rho_L \beta_c (c - c_0) g \mathbf{e}_z - \sigma_E B^2 (v_\mathbf{r} \mathbf{e}_r + v_\theta \mathbf{e}_\theta) \tag{5}$$

Table 1: Parameters used in the simulation: *Yildiz and Dost(2005), and **Yildiz, Dost, and Yildiz (2006)

Parameter	Value
Diffusion coefficient: D_{Si}	2.5×10^{-8}m^2/s *
Solutal expansion: β_c	0.0053 *
Liquid density: ρ_L(Ge)	5633 kg/m^3 *
Viscosity: μ(Ge)	7.35x10^{-4} kg/m.s *
Liquid thermal conductivity: k_L(Ge)	42.8 W/m.K *
Liquid specific heat: γ_L(Ge)	380 J/kg.K *
Liquid electric conductivity: σ_E(Ge)	$1.7 \times 10^6 1/\Omega$.m **
Magnetic field intensity: B	8 kGauss

3.2 Initial and boundary conditions

Dissolving boundary (dissolution interface) is taken as saturated in silicon according the phase diagram. The thermal field evolves from the 800˚C initial temperature to the 1100˚C final temperature (the growth temperature used in LPD). The effect of thermal expansion was neglected in Eq.(5) for the present simulation since our previous thermal analysis has shown that the system comes to thermal equilibrium quickly, less than 90 seconds, over the 20min simulation time (Armour and Dost(2007, 2009)). We also checked that the inclusion of thermal expansion did not have notable effect on the flow and concentration fields. The parameters used in the simulation are listed in Tab. 1.

The boundary and initial conditions used in the simulation can be summarized as follows.

Temperature field

Outside quartz tube: $T = 800°C$ at $t = 0$ and $T = 1100°C$ at $t > 0$.

Along the boundaries (the ampoule vertical wall and bottom plane, and the silicon-germanium interface) continuity of heat flux: $k_L \frac{\partial T}{\partial n} = k_S \frac{\partial T}{\partial n}$.

Flow velocity

No slip boundary conditions along the domain boundaries: $v_r = v_\theta = v_z = 0$.

Concentration field

At the dissolving interface silicon mass fraction is determined at the saturated concentration by (Yildiz, Dost and Lent(2005))

$$c_{dis} = 1 - (1.05513 \times 10^{-8} T^3 - 3.446005 \times 10^{-5} T^2 + 0.038741 T - 14.749675).$$

Along the remaining domain boundaries: no mass flux leads to $\partial c / \partial n = 0$.

4 Results and discussion

The dissolution process in the system considered here, in the absence of an applied magnetic field, proceeds under almost isothermal conditions (no temperature gradient). Dissolved silicon species from top source diffuse into the Ge melt under almost convection-free conditions. This is due to the buoyancy of the lighter silicon species in the heavier germanium melt. This stabilizes the melt against convective flow (see Yildiz, Dost and Lent(2005) for details). The sample processed without a magnetic field exhibits a flat dissolution interface consistent with a diffusion dominated transport process. Numerical modeling of the system confirms that the system evolves in a diffusion-dominated manner, as seen in Fig. 2.

However, the situation for the sample processed under an 8 kGauss static magnetic field (applied vertically along the crucible axis) is different. The samples exhibit a flat dissolution interface in the center of the sample but the interface significantly cuts back into the silicon source near the crucible wall, as seen in Fig. 3. This clearly shows the effect of the magnetic field on species transport in the melt.

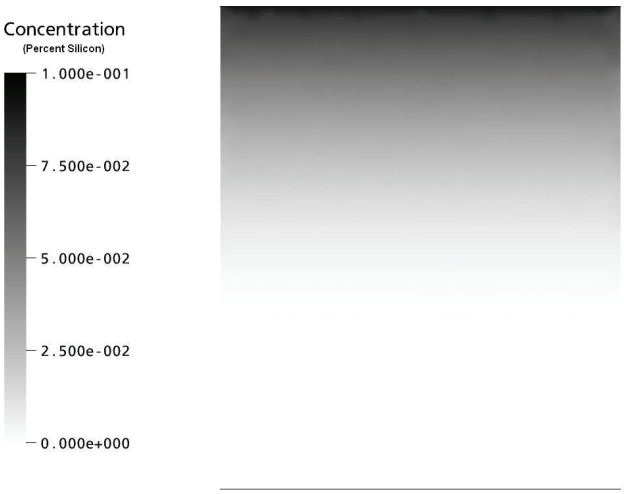

Figure 2: Computed silicon concentration profile (mass fraction) in the melt in the absence of an applied magnetic field. As seen the mass transport is almost diffusion dominated. Dark areas indicate higher silicon concentration. The graph represents six minutes into simulation.

In order to verify the experimental observations, the dissolution process was numerically simulated. The computed flow velocity and concentration fields are presented

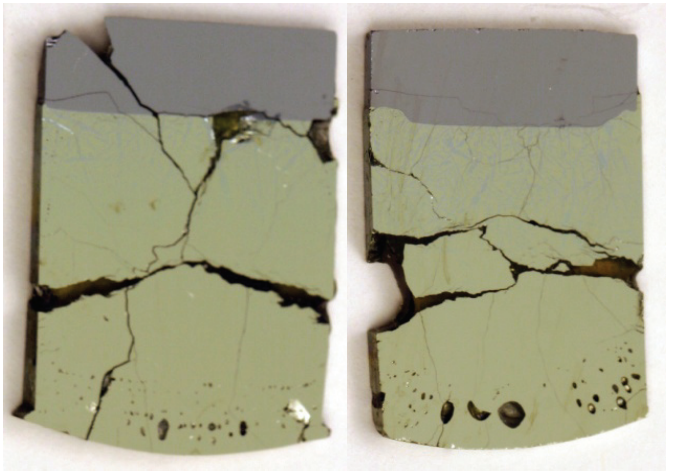

Figure 3: Photographs of the dissolution interface without magnetic field (a) (left) and with the magnetic field (b) (right). The effect of the applied magnetic field is clearly seen on the dissolution near the wall. Samples are 24mm wide.

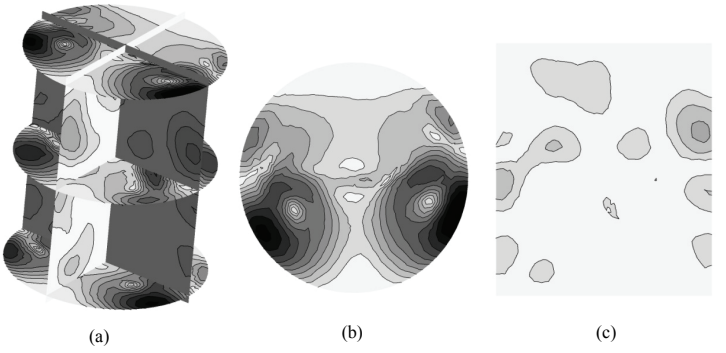

Figure 4: (a) shows an overview of the present 3-D computed flow structure. (b) is the image showing the total velocity magnitude near the dissolution interface. (c) shows the vertical velocity magnitude through the melt in the vertical plane. Darker areas indicate higher velocity and all images use the same color scale. These images are taken at six minutes into the simulation.

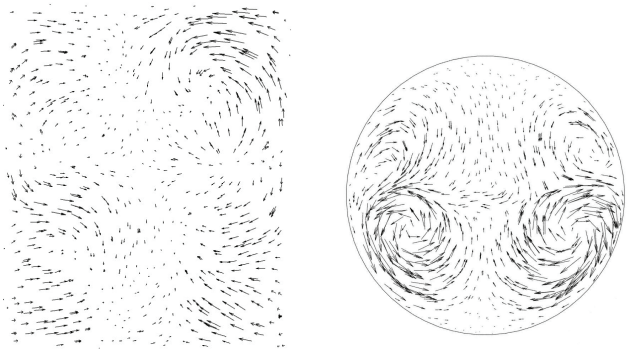

(a) (b)

Figure 5: The left (a) image shows the velocity vectors through the vertical axis of the crucible. The right (b) image shows the velocity vectors around the dissolution interface. These images are taken at six minutes into the simulation.

in Figs. 4 and 5, and Figs. 6 and 7 respectively. The fields are three dimensional as expected. Flow cells are developed in the radial-tangential plane of the crucible (Figs. 4b and 5b). Relatively weaker flow structure develops along the crucible vertical axis. This is a substantially altered flow velocity field with the presence of the applied static magnetic field as predicted from previous experimental results (Armour and Dost(2007, 2009)).

The notable change in the flow field near the edge of the crucible, as seen in Figs. 4a-b, results in concentration profiles driving faster dissolution near the crucible wall (Fig. 6). The computed concentration field is consistent with the altered flow structure. The simulation shows that silicon is being mixed away from the edges of the crucible and into the middle of the melt, as seen in Fig. 7. This leads to a low concentration gradient in the center of the melt and a high gradient around the crucible edge. This type of concentration distribution would result in the interface shape observed experimentally (see sample cross sections in Fig. 3).

The modified flow structure, simulated for the system with applied magnetic field, appears to be the cause for the modified concentration profile seen in the simulation of the system with applied field. The effect of the induced magnetic body forces on the melt is to produce the modified flow structure and therefore the modified concentration profile. In the present experimental set up, the addition of magnetic body forces in the melt changes the diffusion-dominated nature of the system and enhances mixing in the melt contrary to what has been observed in many other systems under applied magnetic fields.

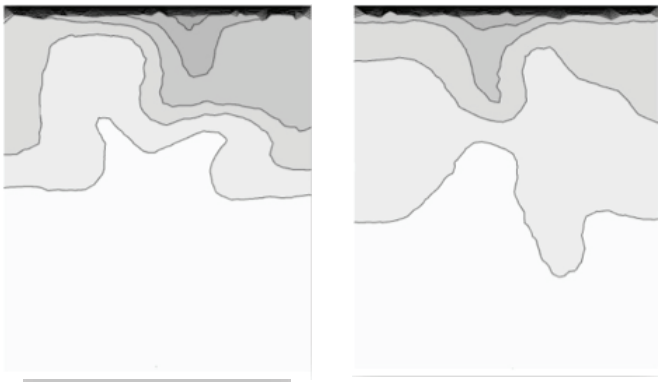

(a) (b)

Figure 6: The left (a) image and the right (b) image are taken through the melt at 90 degrees to one another. The darker areas represent higher silicon concentration. The images are taken at six minutes into the simulation. A higher concentration gradient around the interface is present at the sides relative to the center.

The numerically predicted additional mixing would result in more transport of material and more silicon dissolution as observed in experiments (Armour and Dost(2007, 2009)). The EDS composition measurements of the processed samples presented in Fig. 8 verify the qualitative numerically predicted enhanced transport in the melt. This observation appears to be a characteristic of the Si-Ge system and may be related to the strength of solutal buoyancy in this material system.

5 Conclusion

The additional mixing incurred by applying a static magnetic field could be useful in LPD growth of Si_xGe_{1-x}. The enhanced transport could aid in producing faster growth rates. However, the stability of the growth system (interfaces and flow structures) may be compromised by the altered flow structure.

Although the measured concentration profiles from the samples processed with and without the application of magnetic field showed very similar shape, the amount of silicon transport into the melt is slightly higher in the samples processed under magnetic field. In the presence of an applied field, the dissolution interface remains flat in the center but dramatically curves back into the source material near the wall. This indicates a far higher dissolution rate at the edges of the silicon source.

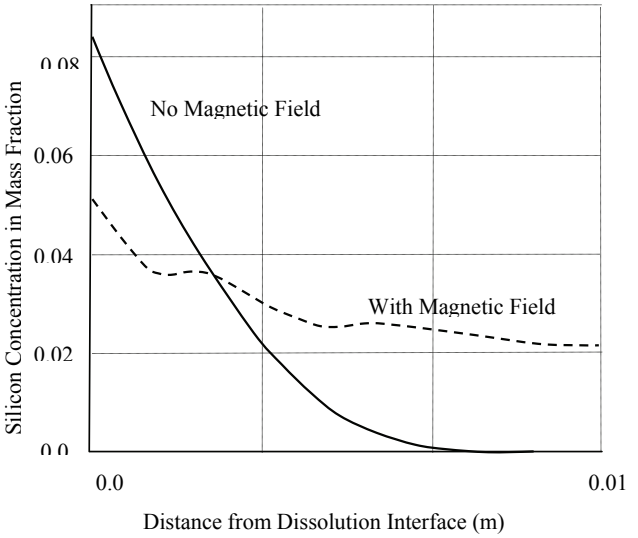

Figure 7: The plot shows the difference in concentration profile between the simulation with and without applied magnetic field. The profiles are taken down the center of the melt. The shallower and varying concentration profile with applied field shows the effect of convection.

The 3-D numerical simulation results verify these observations and show that the flow structure of the melt in the present system has dramatically changed under the effect of magnetic field. Flow cells develop at the edge of the melt affecting dissolution from these areas. Silicon transport is enhanced near the crucible wall.

Our future studies will examine the evolution of the concentration profile near the growth interface in the LPD growth of Si_xGe_{1-x} single crystals through both experiments and numerical simulations. This would determine how uniform the growth would proceed and how the growth interface shape would evolve. The present results obtained from the dissolution process does not provide sufficient information on how uniform the long range transport of silicon will be across at a given cross section of the melt.

For Melt-Replenishment Czochralski, where a typical configuration would have the dissolution interface at the crucible edge and growth interface in the center (same surface), the applied magnetic field could be particularly useful. Specifically, the mixing of the species from the edge into the center could enhance transport of silicon to the growth interface and allow for faster pulling rates. Again, the effects of the altered flow structure on growth stability would need to be investigated further

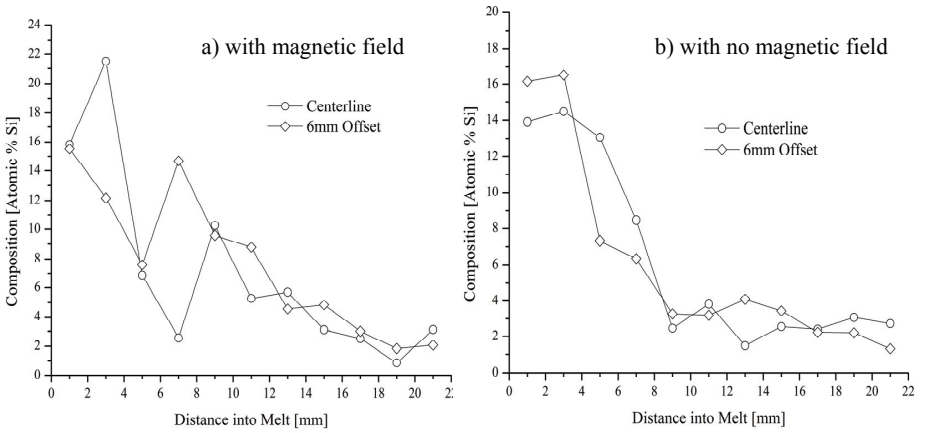

Figure 8: The left plot (a) is of the measured silicon concentration (EDS) from the sample processed under magnetic field. The right plot (b) is measured concentration profile of the sample processed without the applied field. There is a higher concentration of silicon deeper into the melt in the plot on the left, the sample processed with the magnetic field.

through Cz growth experiments and numerical simulations.

Acknowledgement: The financial support provided by the Canadian Space Agency (CSA), the Natural and Engineering Science Council of Canada (NSERC), and the Canada Research Chairs Program is gratefully acknowledged. The EDS characterization of samples was obtained using the facility at the Karen Kavanagh Laboratory of Simon Fraser University, Burnaby, BC, Canada. We express our appreciation for the availability of the facility.

References

Armour, N.; Dost, S. (2007): The Effect of a Static Magnetic Field on Buoyancy-Aided Silicon Dissolution into Germanium Melt. *J. Crystal Growth*, vol. 306(1), pp. 200-207.

Armour, N.; Dost, S. (2009): Effect of an Applied Static Magnetic Field on Silicon Dissolution into a Germanium Melt. *J. Crystal Growth*, vol. 311, pp. 780–782.

Armour, N.; Dost, S.; Lent, B. (2007): Effect of Free Surface and Gravity on Dissolution in Germanium Melt. *J. Crystal Growth*, vol. 299, pp. 227-233.

Dost, S.; Lent, B. (2007): *Single Crystal Growth of Semiconductors from Metallic Solutions*, Elsevier, Amsterdam, Netherlands.

Kasper, E. (1995): Prospects of SiGe heterodevices. *J. Crystal Growth*, vol. 150, pp. 921-925.

Schuppen, A.; Dietrich, H. (1995): High speed SiGe heterobipolar transistors. *J. Crystal Growth*, vol. 157, pp. 207-214.

Usami, N.; Kitamura, M.; Obara, K.; Nose, Y.; Shishido, T.; Nakajima, K. (2005): Floating zone growth of Si-rich SiGe bulk crystal using pre-synthesized SiGe feed rod with uniform composition. *J. Crystal Growth*, vol. 284, pp. 57-64.

Volz, M.P.; Schweizer, M.; Kaiser, N.; Cobb, S.D.; Vujisic, L.; Motakef, S.; Szofran, F.G. (2002): Bridgman growth of detached GeSi crystals. *J. Crystal Growth*, vol. 237, pp. 1844-1848.

Volz, M.P.; Walker, J.S.; Schweizer, M.; Cobb, S.D.; Szofran, F.R. (2005): Bridgman growth of germanium crystals in a rotating magnetic field. *J. Crystal Growth*, vol. 282, pp. 305-312.

Yildiz, E.; Dost, S. (2007): The Combined Effect of Rotating and Static Magnetic Fields in Liquid Phase Diffusion Growth of SiGe. *J. Crystal Growth*, vol. 303, pp. 279-283.

Yildiz, E.; Dost, S.; Yildiz, M. (2006): A Numerical Simulation Study for the Effect of Magnetic Fields in Liquid Phase Diffusion Growth of *SiGe* Single Crystals. *J. Crystal Growth*, vol. 291, pp. 497-511.

Yildiz, M.: Dost, S. (2005): A Computational Model for the Liquid Phase Diffusion Growth of SiGe Single Crystals. *Int. J. Engng. Sci.*, vol. 43, pp. 1059-1080.

Yildiz, M.; Dost, S.; Lent, B. (2005): Growth of Bulk SiGe Single Crystals by Liquid Phase Diffusion. *J. Crystal Growth*, vol. 280, pp. 151-160.

Yonega, I. (2005): Growth and fundamental properties of SiGe bulk crystals. *J. Crystal Growth*, vol. 275, pp. 91-98.